MATERIALS PHYSICS AND MECHANICS RESEARCH ARTICLE

Submitted: September 1, 2025 **Revised: October 28, 2025** **Accepted: November 12, 2025**

Effect of welding parameters and response surface method based on prediction of maximum temperature generated during friction stir welding of AA3003

A. Belaribi [1], I. Chekalil [2], A. Miloudi [1]✉, M.A. Ben Messaoud [1], A. Zoukel [3]

[1] University of Djillali Liabes, Sidi Bel Abbès, Algeria

[2] King Fahd University of Petroleum and Minerals, Dhahran, Saudi-Arabia

[3] University of Laghouat, Laghouat, Algeria

✉ miloudidz@yahoo.fr

ABSTRACT

Friction stir welding generates significant temperature increases, leading to microstructural changes that influence the mechanical properties of the material. Temperature control is therefore essential to ensure the quality of the welded joint. This study aims to model and predict the maximum temperature generated during the friction stir welding of aluminum alloy 3003, based on three key operating parameters: rotation speed, feed rate, and tool inclination angle. The response surface method was used to develop a robust predictive model and evaluate the individual and combined effects of these parameters on the thermal response. The results reveal that the most influential parameters are, in order, rotation speed, tool inclination angle, and feed rate. They also indicate that the maximum temperature increases significantly with rotational speed and angle of inclination. In contrast, it decreases as the feed rate increases. The model obtained has excellent predictive power, validated by a low root mean square error of 4.41 °C and a coefficient of determination R^2 of 0.972.

KEYWORDS

FSW • T_{max} • RSM • prediction • rotation speed

Citation: Belaribi A, Chekalil I, Miloudi A, Ben Messaoud MA, Zoukel A. Effect of welding parameters and response surface method based on prediction of maximum temperature generated during friction stir welding of AA3003. *Materials Physics and Mechanics*. 2025;53(6): 201–212.
http://dx.doi.org/10.18149/MPM.5362025_15

Introduction

Since the advent of the friction stir welding (FSW) process in 1991 [1], much research has been carried out in both academic and industrial fields for its application in the aerospace sector, and its extension to other sectors and application on other metallic materials such as steel, magnesium and its alloys. In addition to welding, the friction stir welding process has been successfully used to repair cracks [2] and improve material behavior by modifying the microstructure [1–4]. Similarly, FSW welds have significantly higher fatigue strength than other welding techniques [5]. FSW welded assemblies have very good mechanical strength, averaging 80 % of that of the base material [6]. Moreover, the microstructure of the alloys remains little changed compared to liquid phase welding techniques.

This technique uses a non-consumable rotating tool to generate frictional heat, softening materials without melting and producing high-quality, defect-free welds [7–10]. Despite these advantages, achieving better joint quality remains a major challenge. Several

methods have been explored to improve the performance of FSW joints: Underwater friction stir welding (UWFSW) has been applied to AA5083 alloy to improve its mechanical and corrosion resistance [11,12]. At the same time, heat treatments have been used to optimize AA2014-AA7075 heterogeneous joints [13]. These two approaches have resulted in tensile strengths and hardnesses exceeding those of conventional processes, highlighting the crucial role of thermal control on the final performance of joints.

Peak temperature in the weld zone significantly affects weld quality, as excessive temperatures can dissolve precipitates in precipitation-hardened alloys, leading to reduced mechanical properties [14,15]. Typical FSW peak temperatures for aluminum alloys range from 200–550 °C depends on process parameters. The temperature rise during FSW welding leads to microstructural changes that influence the material properties. Temperature control is therefore essential to guarantee the quality of the welded joint. Accurate prediction of this temperature ensures optimal weld strength and minimizes defects [14].

Numerous studies have focused on predicting the rate of heat generation and maximum temperature during friction stir welding (FSW), intending to assess the quality of the resulting joints. Khalifa et al. [16] predicted the FSW temperature of 6061 T6 aluminum. They showed that welding speed is responsible for 63 % of the temperature variation. Selvaraj [17] used a regression model to predict peak temperature during friction stir welding of steel. The results showed that the peak temperature reached is related to rotational speed (*N*) and inversely proportional to welding speed (*S*).

Using finite element modeling, Meyghani et al. [18] investigated the influence of the friction coefficient on thermal behavior during friction stir welding (FSW). Their results showed that the temperature reached during the process is directly impacted by the value of this coefficient. In the same context, Palanivel et al. [19] developed a finite element (FE) model to predict temperature distribution during friction stir welding (FSW). The results show that simulated values deviate from experimental measurements by around 3 %.

Chamoret et al. [20] have developed a 3D nonlinear thermal model to simulate the thermal history during FSW welding of AISI 316L. The simulated temperature distributions were compared with experimental values and showed good agreement.

The studies presented above demonstrate that welding speed has a significant impact on heat generation and peak temperature during friction stir welding (FSW), while the effect of tool penetration and the interaction between these parameters has not been sufficiently investigated.

Other studies suggest that rotation speed most significantly affects peak temperature during FSW, followed by welding speed and axial force. Increasing rotational speed boosts frictional heat generation, raising peak temperatures, while higher welding speeds decrease heat input per unit length, leading to lower temperatures. For example, in FSW of AA6061, Dadi et al. [21] and Meyghani et al. [22] reported peak temperatures ranging from approximately 300 to 467.4 °C under different process parameters. Specifically, a minimum temperature of about 300 °C was observed at 600 rpm, 130 mm/min, and a constant axial force of 3 kN, while the maximum of 467.4 °C was reached at 1200 rpm, 70 mm/min, and a constant axial force of 7 kN. These findings emphasize the key role of rotational speed in controlling temperature when axial force is systematically varied or kept constant within the experimental setup.

Saravanakumar et al. [23] examined the influence of the rotation speed/feed speed ratio (*N*/*S*) on weld quality. Their results showed that an increase in this ratio led to an increase in the maximum temperature during welding. This increase in temperature caused the core and core zone to widen, leading to a reduction in joint hardness.

Response surface methodology (RSM) is the most widely used soft computing technique for modeling the performance parameters of the FSW process. It develops second-degree polynomial regression equations to predict these parameters [24]. RSM has been crucial in estimating the performance of aluminum alloy welding, including yield strength [25], elongation [26,27], weld joint hardness [28], ultimate tensile strength (UTS) [26,29–31], among others. For AA6061-T6, a thermo-mechanical model using RSM predicted a peak temperature of ~ 453 °C under stable welding conditions, validated with experimental data [32].

The AA3003 alloy is frequently used in oil storage and gasoline transportation systems, heat exchangers, and marine equipment. Its light weight and good corrosion resistance make it a material of choice for manufacturing components such as automotive evaporators and radiators.

Numerous studies have explored the effect of welding parameters on the mechanical strength of AA3003 alloy joints welded by FSW. Chekalil and Miloudi [33] studied the effect of rotation speed, feed rate, and tool inclination angle on the mechanical strength of friction stir-welded (FSW) joints in AA3003 alloy. However, no study has yet evaluated the combined effect of these parameters on the thermal evolution during welding of this alloy. Continuing this work, we maintained the same welding conditions to analyze their influence on the temperature evolution during the FSW process.

In this article, the effect of three main parameters, namely the tool rotation speed (*N*), the feed rate (*S*), and the angle of inclination (θ), on the maximum temperature generated during friction stir welding of AA 3003 aluminum was investigated using the response surface method (RSM) with 27 experiments in the factorial design. The equation obtained makes it possible to predict the maximum temperature based on these parameters.

Methods

The friction stir welding tool was manufactured from X210Cr12 steel with a breaking strength of σ_m = 870 MPa, selected based on preliminary tests conducted by Chekalil and Miloudi [33] on the tool itself to validate the design. The chosen geometry is similar to that of a conical pin, with the following dimensions: d = 5 mm, D = 6.8 mm, and length = 1.7 mm. It features a concave shoulder with a 3° angle and a diameter of 19.5 mm.

Two AA3003 aluminum alloy plates with dimensions 210 × 110 × 2 mm^3 were butt-welded along the rolling direction (RD) in a single pass using friction stir welding (FSW). The mechanical characteristics of aluminum alloy 3003 were determined by tensile tests carried out on an INSTRON 8500 servo-hydraulic machine with a capacity of ± 100 kN. The rational curve for the alloy is shown in Fig. 1. This test was used to determine the main mechanical characteristics of the base material, which are listed in Table 1.

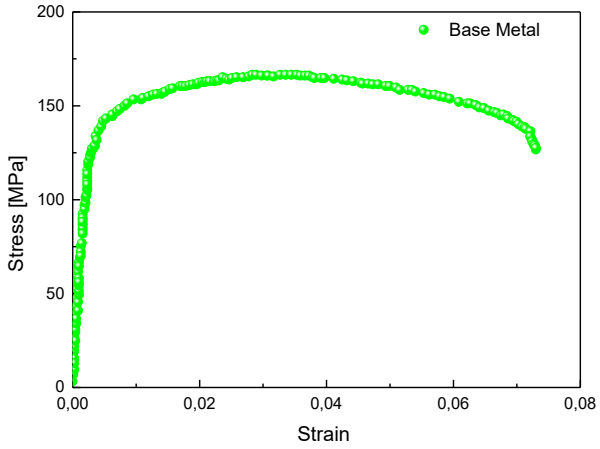

Fig. 1. Rational curves of the tensile test for aluminium alloy 3003

Table 1. Mechanical properties of the material before welding (σ_e is yield stress, σ_U is ultimate tensile strength, σ_m is rupture strength, *A* is elongation, *E* is the Young modulus)

Microhardness, HV	σ_e, MPa	σ_U, MPa	σ_m, MPa	*A*, %	*E*, GPa
51.0	130.0	160.0	127.0	5.6	60.0

Chekalil et al. [34] characterized the different microstructural zones of an AA 3003 FSW joint under the same welding conditions. This analysis was carried out under optimal welding conditions (*N* = 1400 rpm, *S* = 400 mm/min, and θ = 1.5°).

The chemical composition of the alloy was determined by A COXEM scanning electron microscope (SEM) with 15Kv voltage and x2000 magnification. Table 2 represents the chemical composition of the material used.

Table 2. Chemical composition of aluminum alloy 3003

Element	Al	Mn	Si	Fe	Cu	Ti	Zn	Mg	Cr
%	96.7	1.3	0.9	0.9	0.13	0.1	0.03	0	0

We note that the welded joint presents a very heterogeneous microstructure. Indeed, the thermal gradient and the deformation gradient imply a gradient of the microstructures across the weld. The micrographs observation in the direction orthogonal to the welding direction allowed us to distinguish 4 main zones. The core is located in the center of the weld. In this zone the grain size is the finest with an equi-axial shape thanks to the deformation generated by the pin. The ZATM (thermo-mechanically affected zone) is close to the core, reveals elongated grains with a relatively large size. This reformulation is caused by the flow of materials around the pin and below the shoulder. The ZAT (thermal affected zone) is characterized by large grains with an equi-axial geometry. This coarsening is the result of the heat flow generated by the tool. Finally, the base metal is recrystallized and presents an equi-axial grain structure.

The design of experiment was used for the statistical design of the tests. The three process parameters considered were rotation speed N (rpm), feed rate S (mm/min), and tilt angle θ (°). Table 3 below shows the values of each parameter for each level. The maximum temperature T_{max} (°C) reached during welding was chosen as the main response variable to measure the thermal impact of the process.

Table 3. Parameter values for each level

Parameter	Level 1	Level 2	Level 3
N, rpm	1000	1500	2000
S, mm/min	100	200	400
θ, °	0.5	1.5	2.5

The FSW welding operation is carried out in conjunction with a thermal characterization procedure, which involves the measurement of temperatures on both sides of the joint: advance (AS) and retract (RS), temperature evolution was monitored using Type-K thermocouples with a temperature capability ranging from -40 to 1200 °C and connected to a thermal recorder, which will be installed on the sheets, at a distance of 2 and 4 mm from the center of the joint, using Thermigrease TG 20033 thermal paste to ensure optimum heat transfer. The positioning of the thermocouples and sampling are illustrated in Fig. 2.

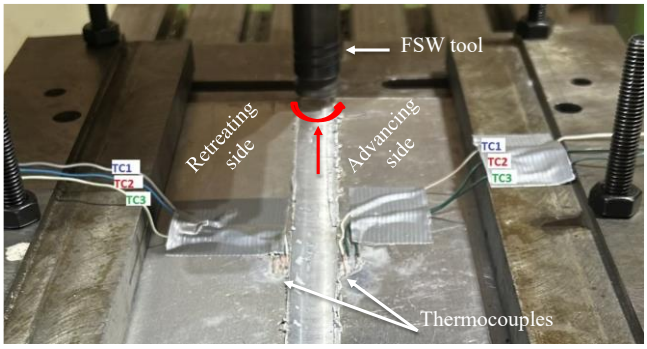

Fig. 2. Thermocouple and sampling positioning

Figure 3 illustrates the evolution of the thermal cycle in the forward (AS) and reverse (RS) directions. Examination of this figure reveals a rapid increase in temperature as the tool approaches the thermocouple, and a slow decrease as it moves away from it. This evolution is observed independently of the position of the thermocouple. In addition, it has been observed that the temperature gradient intensifies significantly the closer one gets to the center of the weld. In addition, it was found that temperatures measured on the advancing side are slightly higher than those on the retreating side, with a difference of up to a few ten degrees.

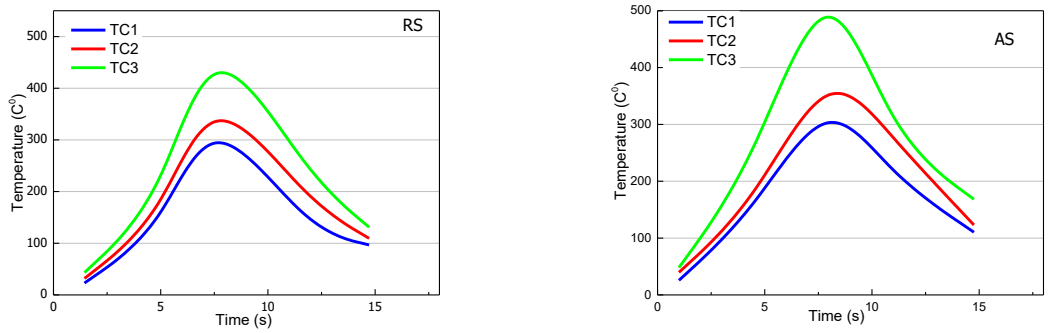

(a) (b)

Fig. 3. Temperature evolution during FSW of alloy 3003 on the advancing (a) and retreating sides (b) at several distances from the weld center

This thermal asymmetry between the advancing (AS) and retreating (RS) sides is a well-known feature of the FSW process [35], associated with the direction of rotation of the tool relative to the workpiece feed. This increased heat dissipation manifests itself mainly on the AS side. All the maximum temperatures analyzed in the rest of this study correspond to measurements taken on the feed side, which is the most thermally stressed zone. The experiment matrix was determined by MODDE 5.0 software, following a 3^3 full factorial design (27 trials). The results of the 27 tests are presented in Table 4.

Table 4. Experimental design results.

N°	N, rpm	S, mm/min	θ, °	T_{max}, °C
1	1000	200	0,5	207
2	1500	200	0,5	242
3	2000	200	0,5	323
4	1000	300	0,5	198
5	1500	300	0,5	221
6	2000	300	0,5	274
7	1000	400	0,5	184
8	1500	400	0,5	200
9	2000	400	0,5	263
10	1000	200	1,5	216
11	1500	200	1,5	254
12	2000	200	1,5	310
13	1000	300	1,5	203
14	1500	300	1,5	239
15	2000	300	1,5	282
16	1000	400	1,5	194
17	1500	400	1,5	213
18	2000	400	1,5	260
19	1000	200	2,5	295
20	1500	200	2,5	342
21	2000	200	2,5	397
22	1000	300	2,5	236
23	1500	300	2,5	300
24	2000	300	2,5	366
25	1000	400	2,5	216
26	1500	400	2,5	272
27	2000	400	2,5	316

Results and Discussion

The polynomial mathematical model developed for optimizing the maximum temperature during FSW welding is a second-degree model of the form:

$$y = a_0 + \sum_{i=1}^{3} a_i x_i + \sum_{1 \le j \le 3} a_{ij} x_j + \sum_{i=1}^{3} a_{ii} x_i^2 + e \quad , \qquad (1)$$

where a_0 is the predicted response value at the center of the experimental range, a_i represents the effect of the factor x_i, and a_{ij} represents the interaction between the factor x_i and x_j.

The mathematical model developed establishes a relationship between the input parameters (N, S and θ) and the output variable (T_{max}). To calculate the model coefficients, a regression method based on the least-squares criterion is used. The

mathematical model proposed by MODDE 5.0 is as follows: $T_{max} = 3{,}366664 \times 10^{-5} \times \times N^2 - 0.000111667 \times N \times S + 0.01016668 \times N \times \theta + 0{,}01080576 \times N + +0.000241664 \times S^2 - 0.0875002 \times S \times \theta - 0.1062476 \times S + 27.0833 \times \theta^2 - -35.36096 \times \theta + 212.270165$.

The values of the coefficients associated with the maximum welding temperature parameters in the mathematical model show the degree of influence of each factor. Model (1) was used to predict the evolution of T_{max} as a function of the input parameters (N, S and θ) as shown in Fig. 4 below, where the central curves represent the predicted values, and the other two curves show the 95 % confidence interval of the predicted response.

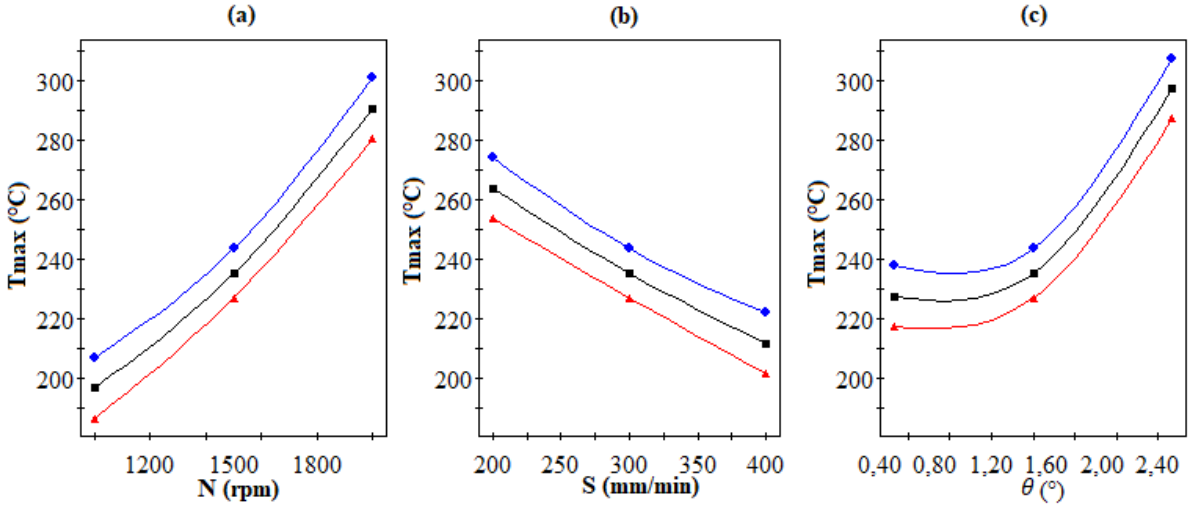

Fig. 4. Evolution of predicted T_{max} as a function of welding parameters

Analysis of Fig. 4(a) suggests that an increase in rotation speed N leads to a sharp rise in T_{max}. Indeed, a 100 % increase in rotational speed leads to an increase of around 155 % in T_{max}. This temperature is highest when the speed is equal to 2000 rpm. On the other hand, it is minimal for low values of N. This correlation can be explained by the fact that higher rotational speeds cause greater mechanical deformation and generate more heat through friction. This heating reduces the mechanical strength of the alloys and increases their ductility.

Figure 4(c) illustrates the effect of inclination angle on T_{max}. It can be clearly seen that T_{max} is constant in the interval between 0.5° and 1.5°, after which T_{max} increases with increasing θ. The maximum value of T_{max} is obtained at an angle of 2.5°. This inclination increases the force applied to the trailing edge of the tool, which contributes to raising the temperature.

Concerning the impact of feed speed, Fig. 4(b) shows that as S increases, T_{max} decreases. A 100 % increase in feed speed results in an 18 % decrease in maximum temperature. Furthermore, it can be observed that the temperature is lowest for extreme values of S, whereas T_{max} is recorded for low values S, which is contrary to the results previously published by Mimmi et al. [36]. In fact, a low feed rate increases contact time and heat input, resulting in more intense and prolonged heating. This heat is essential

to reach the optimum plasticity temperature, which allows complete plastic flow of the material and eliminates critical interface defects such as kissing bonds.

In this stage of the analysis, we expand our comments by considering the interaction between two factors while keeping the third constant. The response variation of T_{max} is visualized as Iso curves in Fig. 5.

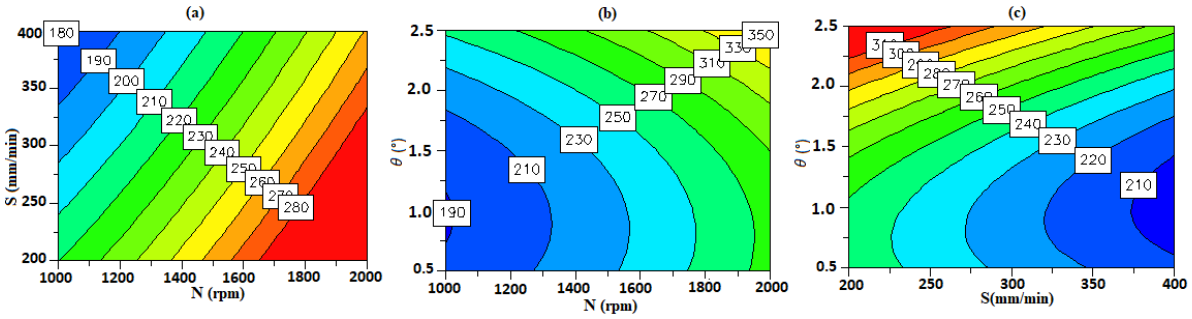

Fig. 5. Prediction of T_{max} as a response to two factors interaction

Figure 5(a) shows the effect of the two factors S and N acting simultaneously on T_{max}, moving from their minimum to their maximum values, while the third factor (θ) is kept constant. Analysis of the graph in this figure suggests that as N increases, T_{max} also increases until it reaches the maximum value of 280 °C, while S lies between 200 and 320 mm/min. On the other hand, low T_{max} values are recorded for low N values around 1000 rpm and high S values between 340 and 400 mm/min.

Concerning the impact of rotation speed and tilt angle on T_{max}, Fig. 5(b) shows that as N increases, T_{max} rises to reach a maximum value of 350 °C. It can also be seen that T_{max} is at its highest for extreme values of θ. On the other hand, low values of T_{max} are recorded for low values of N and θ; they are recorded for values of N between 1000 and 1300 rpm, and θ between 0.5 and 1.2°.

Figure 5(c) illustrates the variation of T_{max} as a function of S and θ. Analysis of this curve shows that maximum temperatures are reached at a feed speed of between 200 and 260 mm/min and a rotation angle of between 2.2 and 2.5°. On the other hand, low values are reached at high feed speeds and low rotation angles, in the range [380–400 mm/min] and [2.2–2.5°], respectively. Consequently, it can be concluded from this analysis that a maximum value of T_{max} is obtained for a value of N between 1650 and 2000 rpm, while keeping the value of S constant between 340 and 400 mm/min.

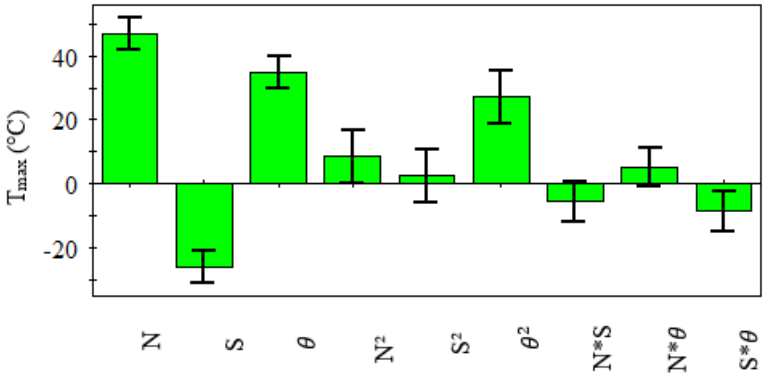

Fig. 6. Parameters with the greatest influence on T_{max}

In order to identify the parameters that have the greatest influence on the maximum temperature generated during welding, an analysis of variance (ANOVA) was performed based on the model established using the response surface methodology (RSM). This approach allows for a quantitative assessment of the individual impact of each factor, as well as their interaction and quadratic effects. The results of this analysis are summarized in Fig. 6, which highlights the relative contributions of the different terms in the model.

Statistical analysis has shown that the most influential parameter is rotational speed, while tilt angle is less important, and feed rate has the least influence. In other parts, the model coefficients allow us to evaluate the interaction effect between the different factors of the process and the response. We note that the factors (N,θ) are the most significant. On the other hand, the factors (N,S) and, as well as (θ,S) are the weakest. We can also note that the effect of the coefficients following S^2 is negligible.

Model validation is a fundamental step in experimental design. It involves comparing the maximum values of the measured temperatures with the responses calculated by the model. As shown in Fig. 7, the more the points are aligned with the first bisector, the higher the descriptive quality of the model. The root-mean-square error (RMSE) is 8.84°C, and the estimates are generally conservative. However, the results obtained by the model are closer to reality.

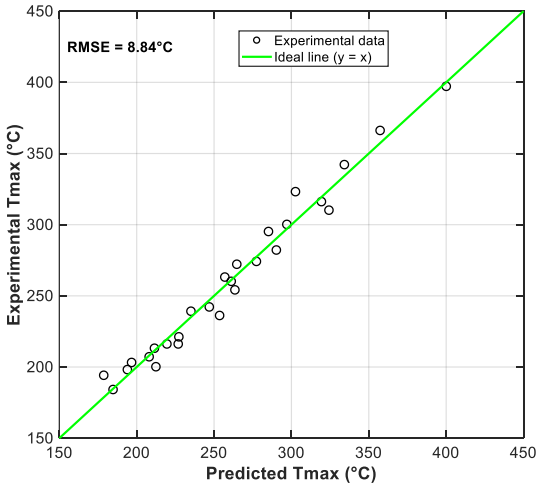

Fig. 7. Model performance

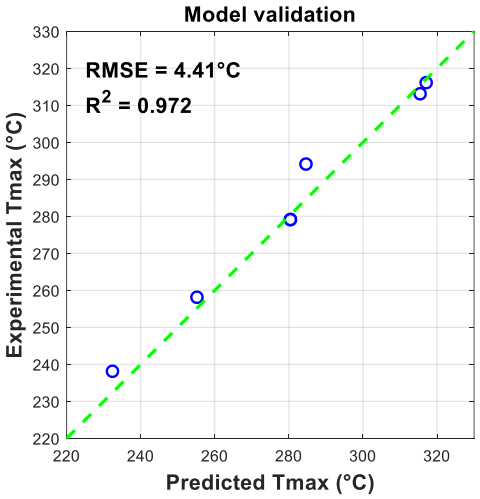

Fig. 8. Model validation

This second step allows us to study the generalization qualities of the proposed model, meaning its predictive behavior. Six additional experimental tests were carried out. The conditions for these tests were randomly selected within the variation ranges of the process parameters. Figure 8 illustrates a comparison between the six experimental results and those predicted by the proposed model.

Figure 8 demonstrates that the results obtained using the proposed model are in agreement with the experimental results, even when compared to those of the RSM model development. The model therefore provides a better prediction of the maximum temperature generated during FSW welding of aluminum alloy AA3003. This is confirmed by a coefficient of determination R^2 of 0.972 and a low root-mean-square error (RMSE) of 4.41 °C.

After studying the generalization of the model, a stage of optimizing these parameters becomes more interesting. This involves determining the optimum values for the tool's rotational speed (*N*), feed rate (*S*), and angle of inclination (θ) (Table 5). These three factors contribute to improving the quality of the FSW joint. These values are obtained by maximizing YS, UTS, and RS [33]. The optimum parameters identified were *N* = 1.423.93 rpm, *S* = 400 mm/min, and θ = 1.2885°. This analysis step identifies the maximum temperature during FSW welding of AA 3003 and ensures that it remains compatible with achieving good mechanical performance.

Table 5. T_{max} for optimal process parameters

N, rpm	S, mm/min	θ, °	σ_U, MPa	σ_e, MPa	σ_m, MPa	T_{max}, °C
1087.13	399.997	0.7508	116.771	49.9487	83.489	182.15331
1685.85	200.015	1.3552	122.24	41.8872	91.1325	278,262731
1694.02	200	1.281	122.59	41.7067	91.047	276.562232
1900	400	2.0999	122.156	39.5626	86.7125	277.875911
1423.93	400	1.2885	121.186	55.3134	94.6581	201.440827
1799.9	200	1.4948	122.716	41.8335	89.989	297.858791
1600	400	1.5	118.225	42.2038	94.8028	220.242196

For these optimum values, the corresponding maximum temperature is 201.44 °C. Figure 9 shows the various possible combinations of rotational speeds, feed rates, and angles of rotation to achieve this temperature.

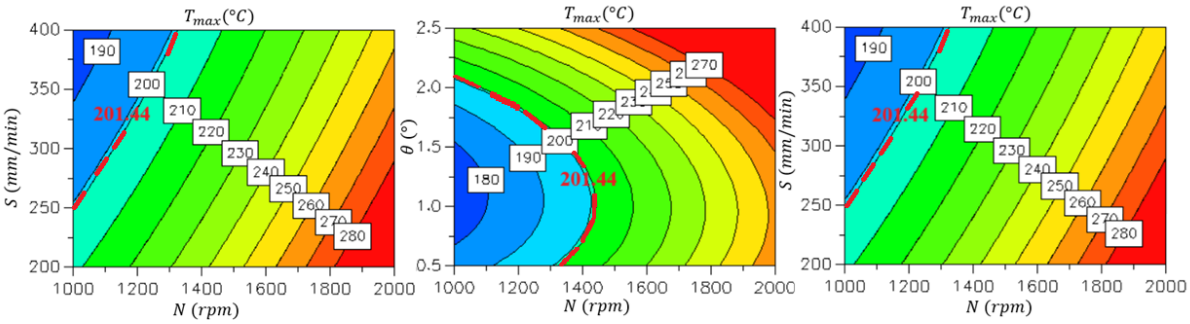

Fig. 9. T_{max} corresponding to the optimal values

Conclusion

The aim of our study is therefore to develop a mathematical model using response surface methodology (RSM). This model enables the prediction of the maximum temperature generated during FSW welding of AA3003 alloy as a function of rotational speed, feed rate, and tool inclination angle. It also enables the effect of these parameters on the evolution of the maximum temperature to be determined.

The model developed enabled us to obtain a better prediction of T_{max}. This model is an effective tool for selecting optimum FSW process parameters. Statistical analysis has shown that the most influential parameter is rotational speed, while tilt angle is less important, and feed rate has the least influence. Although response surface methodology

(RSM) is simple to implement and has a low computational cost, it is important to explore new approaches, such as artificial intelligence methods, to minimize prediction error.

CRediT authorship contribution statement

Belaribi Amina: writing – review & editing, writing – original draft, data curation; **Chekalil Ismail:** data curation, investigation, writing – review & editing; **Miloudi Abdelkader:** conceptualization, data curation, writing – original draft; **Ben Messaoud Mohamed Abdelghani:** data curation, writing – review & editing; **Zoukel Abdelhalim:** supervision.

Conflict of interest

The authors declare that they have no conflict of interest.

References

1. Mishra RS, Ma ZY. Friction stir welding and processing. *Materials Science and Engineering R: Reports.* 2005;50(1–2): 1–78.
2. Masroor Z, Rauf AA, Mustafa F, Hussain SW. Crack Repairing of Aluminum Alloy 2024 by Reinforcement of Al_2O_3 and B_4C Particles using Friction Stir Processing. In: *2019 Sixth International Conference on Aerospace Science and Engineering (ICASE), Islamabad, Pakistan, 2019*. IEEE; 2019. p.1–6.
3. Nasiri Z, Sarkari Khorrami M, Mirzadeh H, Emamy M. Enhanced mechanical properties of as-cast Mg-Al-Ca magnesium alloys by friction stir processing. *Materials Letters.* 2021;296: 129880.
4. Nouri Z, Taghiabadi R, Moazami-Goudarzi M. Mechanical properties enhancement of cast Al-8.5Fe-1.3V-1.7Si (FVS0812) alloy by friction stir processing. *Archives of Civil and Mechanical Engineering.* 2020;20: 141.
5. Lomolino S, Tovo R, Dos Santos J. On the fatigue behaviour and design curves of friction stir butt-welded Al alloys. *International Journal of Fatigue.* 2005;27(3): 305–316.
6. Ma YE, Xia ZC, Jiang RR, Li WY. Effect of welding parameters on mechanical and fatigue properties of friction stir welded 2198 T8 aluminum–lithium alloy joints. *Engineering Fracture Mechanics.* 2013;114: 1–11.
7. Yang D, Jiang H, Ai S, Yang T, Zhi Z, Jing D, et al. Detection method for weld defects in time-of-flight diffraction images based on multi-image fusion and feature hybrid enhancement. *Engineering Applications of Artificial Intelligence.* 2024;138: 109442.
8. Merzoug M, Ghazi A, Lousdad A, Benamara N, Miloudi A, Boulenouar A. Effect of the parameters affecting the properties during friction stir welding of AA 5083 H111 alloy. *Materials Physics and Mechanics.* 2023;51(5): 115–125.
9. Mimmi A, Merzoug M, Ghazi A, Dellal N. Mechanical behavior of structures welded with friction stir lap welding process. *Materials Physics and Mechanics.* 2023;51(2): 151–163.
10. Belaziz A, Bouamama M, Elmeguenni Imane, Zahaf S. Experimental study of the roughness variation of friction stir welding FSW. *Materials Physics and Mechanics.* 2023;51(3): 115–125.
11. Saravanakumar R, Rajasekaran T, Pandey C. Underwater Friction Stir Welded Armour Grade AAA5083 Aluminum Alloys: Experimental Ballistic Performance and Corrosion Investigation. *Journal of Materials Engineering and Performance.* 2023;32: 10175–10190.
12. Saravanakumar R, Rajasekaran T, Pandey C. Mechanical and Microstructural Characteristics of Underwater Friction Stir Welded AAA5083 Armor-Grade Aluminum Alloy Joints. *Journal of Materials Engineering and Performance.* 2022;31: 8459–8472.
13. Kumar R, Upadhyay V, Pandey C. Effect of Post-Weld Heat Treatments on Microstructure and Mechanical Properties of Friction Stir Welding Joints of AAA2014 and AAA7075. *Journal of Materials Engineering and Performance.* 2023;32: 10989–10999.
14. Anandan B, Manikandan M. Machine learning approach for predicting the peak temperature of dissimilar AAA7050-AAA2014A friction stir welding butt joint using various regression models. *Materials Letters.* 2022;325: 132879.
15. Sandeep R, Natarajan A. Prediction of peak temperature value in friction lap welding of aluminium alloy 7475 and PPS polymer hybrid joint using machine learning approaches. *Materials Letters.* 2022;308: 131253.

16. Khalifa RB, Toumi O. Prediction of the friction stir welding temperature and ultimate tensil stress for 6061 T6 aluminum. *Journal of Mechanical Engineering Science*. 2025;239(14): 5622–5635.
17. Selvaraj M. Regression model for obtaining peak temperature and heat generation during friction stir welding of stainless steel. *Materials Today: Proceedings*. 2022;62: 633–637.
18. Meyghani B, Awang MB, Poshteh RGM, Momeni M, Kakooei S, Hamdi Z. The Effect of Friction Coefficient in Thermal Analysis of Friction Stir Welding (FSW). *IOP Conference Series: Materials Science and Engineering*. 2019;495: 012102.
19. Palanivel V, Johnson P, Munimathan A, Arumugam ST. Finite element analysis of friction stir welding process to predict temperature distribution. *Revista Materia*. 2024;29(4): e29465.
20. Chamoret D, Lebaal N, Roman A, Schlegel D, Langlade C. Thermal aspects in friction stir process of AISI 316L: Numerical and experimental investigation. *Mechanics of Advanced Materials and Structures*. 2020;27(1): 74–79.
21. Dadi SSO, Patel C, Appala Naidu B. Effect of friction-stir welding parameters on the welding temperature. *Materials Today: Proceedings*. 2021;38: 3358–3364.
22. Meyghani B, Awang M, Wu CS. Finite element modeling of friction stir welding (FSW) on a complex curved plate. *Journal of Advanced Joining Processes*. 2020;1: 100007.
23. Saravanakumar R, Rajasekaran T, Pandey SM, Sirohi S, Pandey C. Effects of welding parameter on the microstructure and mechanical properties of friction stir-welded non-heat treatable alloy AAA5083. *Journal of Adhesion Science and Technology*. 2024;2024: 1–19.
24. Medhi T, Hussain SAI, Roy BS, Saha SC. An intelligent multi-objective framework for optimizing friction-stir welding process parameters. *Applied Soft Computing*. 2021;104: 107190.
25. Elatharasan G, Kumar VSS. An Experimental Analysis and Optimization of Process Parameter on Friction Stir Welding of AA 6061-T6 Aluminum Alloy using RSM. *Procedia Engineering*. 2013;64: 1227–1234.
26. Heidarzadeh A. Tensile behavior, microstructure, and substructure of the friction stir welded 70/30 brass joints: RSM, EBSD, and TEM study. *Archives of Civil and Mechanical Engineering*. 2019;19(1): 137–146.
27. Senthil SM, Parameshwaran R, Ragu Nathan S, Bhuvanesh Kumar M, Deepandurai K. A multi-objective optimization of the friction stir welding process using RSM-based-desirability function approach for joining aluminum alloy 6063-T6 pipes. *Structural and Multidisciplinary Optimization*. 2020;62: 1117–1133.
28. Rathinasuriyan C, Kumar VSS. Optimisation of submerged friction stir welding parameters of aluminium alloy using RSM and GRA. *Advances in Materials and Processing Technologies*. 2020;7(4): 696–709.
29. Jayaraman M, Sivasubramanian R, Balasubramanian V, Lakshminarayanan AK. Prediction of Tensile Strength of Friction Stir Welded A356 Cast Aluminium Alloy Using Response Surface Methodology and Artificial Neural Network. *International Journal of Materials and Structural Integrity*. 2008;9(1–2): 45–58.
30. Rajakumar S, Muralidharan C, Balasubramanian V. Optimization of the friction-stir-welding process and tool parameters to attain a maximum tensile strength of AA7075-T6 aluminium alloy. *Proceedings of the Institution of Mechanical Engineers, Part B: Journal of Engineering Manufacture*. 2010;224(8): 1175–1191.
31. Singh HN, Kaushik A, Juneja D. Optimization of process parameters of friction stir welded joint of AA6061 and AA6082 by response surface methodology (RSM). *International Journal of Research in Engineering and Innovation*. 2019;03: 417–427.
32. Yang T, Wei X, Zhou J, Jiang H, Liu X, Man Z. The Formation Mechanism of Residual Stress in Friction Stir Welding Based on Thermo-Mechanical Coupled Simulation. *Symmetry*. 2025;17: 917.
33. Chekalil I, Miloudi A, Planche MP, Ghazi A. Prediction of mechanical behavior of friction stir welded joints of AA3003 aluminum alloy. *Fracture and Structural Integrity*. 2020;14: 153–168.
34. Chekalil I, Chadli R, Miloudi A, Ghazi A, Planche MP, Mekid S, Raza MS. Effect of corrosion environments on the mechanical properties of friction stir welded aluminum alloy AA3003. *Journal of Materials Research and Technology*. 2024;33: 2353–2364.
35. Li K, Jarrar F, Sheikh-Ahmad J, Ozturk F. Using coupled Eulerian Lagrangian formulation for accurate modeling of the friction stir welding process. *Procedia Engineering*. 2017;207: 574–579.
36. Mimmi A, Merzoug M, Ghazi A. Prediction of the temperature recorded in lap joint at during the friction stir welding. *Engineering Review*. 2023;43: 82–92.